17

Tunable Hollow Optical Waveguide and Its Applications

Mukesh Kumar, Toru Miura, Yasuki Sakurai and Fumio Koyama
Microsystem Research Center, Tokyo Institute of Technology
Japan

1. Introduction

The prime focus of this chapter is a hollow optical waveguide for integrated optics. Starting with a review of various novel hollow waveguide structures, physics and technology of tunable hollow waveguide have been presented with theory and experiments. With the flexible structure of hollow waveguide, a number of tunable optical functions can be realized; some of them are presented in the chapter. After giving a brief review on various hollow waveguides, we describe the basic structure and propagation characteristics of the tunable hollow waveguide. The possibility of two-dimensional (2D) confinement with a 3D hollow waveguide has been discussed. A widely tunable Bragg reflector based on hollow waveguide is then presented and the possibility of on-chip polarization control using 3D hollow waveguide has been discussed which is followed by the description of a novel tapered 3D hollow waveguide Bragg reflector for an adjustable compensation of polarization mode dispersion (PMD). The chapter closes with a discussion on future prospects of using tunable hollow waveguide in reconfigurable integrated photonic circuits and in other applications. The integration Technology for widely tunable hollow waveguide devices has been introduced and a novel hollow waveguide with vertical and lateral periodicity has then been shown with a high index contrast grating which can add extra design flexibility to control the polarizations and can be more fabrication tolerant.

2. Novel hollow waveguides

Guiding light in lower refractive index media has been interesting for many applications. The novel concepts for guiding light in a waveguide of a core of refractive index lower than that of cladding were proposed in form of Bragg fibers [1], Omni waveguides [2], and antiresonant reflecting optical waveguide (ARROW) [3]. Usually, optical guiding is accomplished by confining light to a region with high refractive index surrounded by cladding material with lower refractive index. Hollow waveguide with an air core offer the potential to minimize the dependence of light transmission on air core transparency, thus various hollow waveguide structures such as photonic band-gap fibers have been studied extensively as shown in Fig. 1.

The index of air is lower than those of typical solid cladding materials, thus it is impossible to confine light due to total internal reflections in hollow waveguide structures. Until now, various ways [4-10] to achieve low index guiding have been proposed and demonstrated,

Source: Frontiers in Guided Wave Optics and Optoelectronics, Book edited by: Bishnu Pal,
ISBN 978-953-7619-82-4, pp. 674, February 2010, INTECH, Croatia, downloaded from SCIYO.COM

which include Bragg waveguides (Photonic band-gap waveguide), metallic waveguides, ARROW, and slot waveguide. Recently, silica hollow core photonic band-gap fiber with a minimum attenuation of 1.72 dB/km has been reported [9]. These hollow core waveguides have a lot of advantages including low nonlinearity, low optical damage threshold and strong optical confinement. Thus, there are various applications such as high power lasers/optical guiding, precise micromachining and gas/liquid sensing as shown in Fig. 2 [11-13].

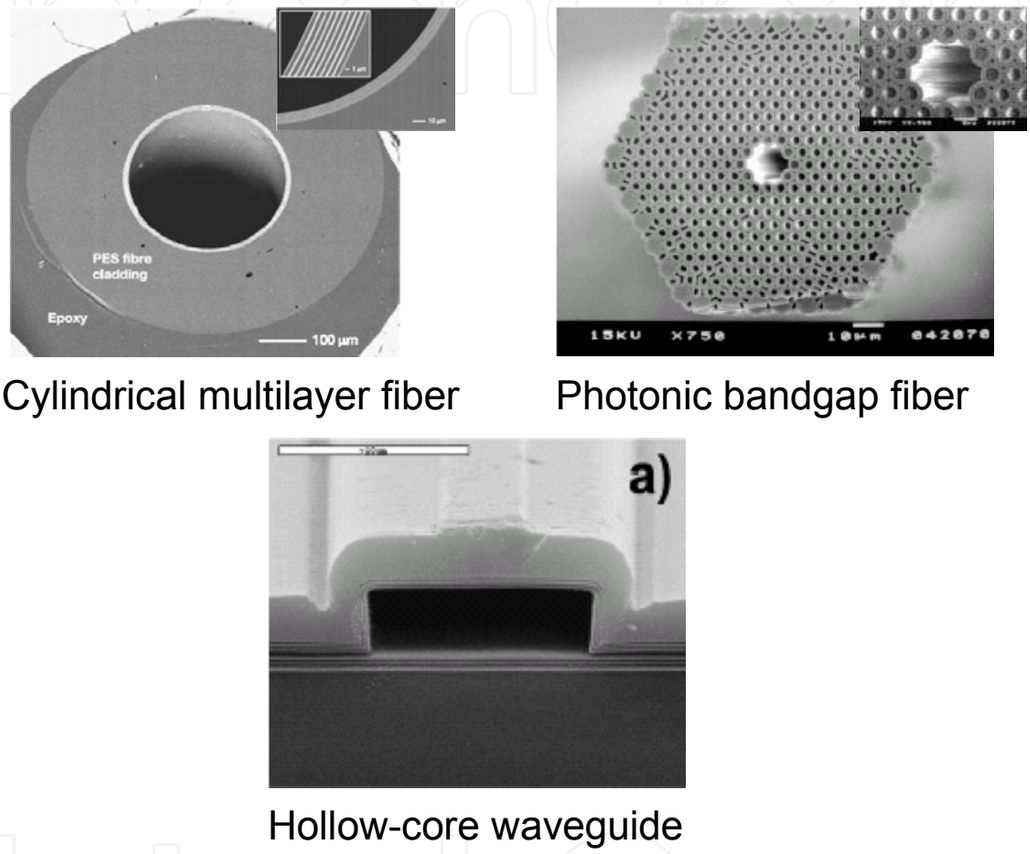

Fig. 1. Various air-core guiding structures [1-3].

Another advantage of hollow core waveguides is temperature insensitivity [7, 14-16]. For many applications in optical fiber communications and sensing, the sensitivity of the phase delay of optical guided mode to temperature is critical and it would be advantageous to decrease this sensitivity. In hollow waveguides, the guided mode is almost entirely confined to the air core region, whereas in a conventional waveguide it is entirely contained in solid materials. Since the temperature dependence of refractive index of air is smaller than that of solid material, the phase delay in hollow waveguides will have much smaller temperature dependence than that in conventional waveguides. In addition, a combination of vertical and lateral periodicities as top and bottom mirrors in hollow waveguide can reduce its polarization dependence [17] and thereby can make it more useful. Also, ultra low-loss hollow waveguide can be realized by using high index contrast grating [18] as top and bottom mirrors with periodicity being in the direction of propagation [19].

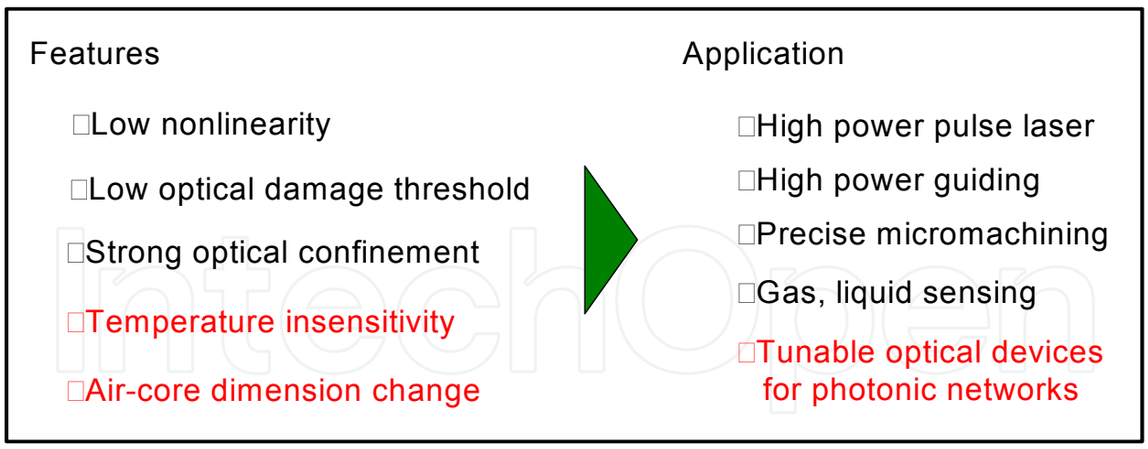

Fig. 2. Application of air-guiding waveguides [11-13].

3. Tunable hollow waveguide

3.1 Tunable and high confinement hollow structure

It has been difficult to utilize the conventional tuning schemes such as thermo-optic or electro-optic effects in hollow waveguides with an air core. Thus, applications to tunable optical devices were hardly discussed at all. In 2001, a novel tunable hollow waveguide structure with variable air core for tunable optical device applications was proposed by T. Miura and F. Koyama [7]. The combination of both hollow waveguides and MEMS actuators enable us to add the tuning functions to hollow waveguides. In tunable hollow waveguides, the light is guided in an air gap between the two multilayer mirrors. Multilayer mirrors with MEMS actuator driven by electrostatic force or thermal bimorph stress bring dynamic mechanical displacement of an air core. The propagation characteristics of hollow waveguide are strongly dependent on air-core dimension, thus one can achieve wide tuning operation of optical properties by air-core dimension control. One-dimensional (1D) and two-dimensional (2D) confinements have been proposed and demonstrated with tunable hollow waveguide structures based on this concept as shown in Fig. 3 [20-23]. In 1D confinement hollow waveguides, vertical confinement of light is achieved by Bragg reflections due to multilayer cladding. To obtain horizontal optical (2D) confinement in 3D hollow waveguides, we use total internal reflections due to effective refractive index

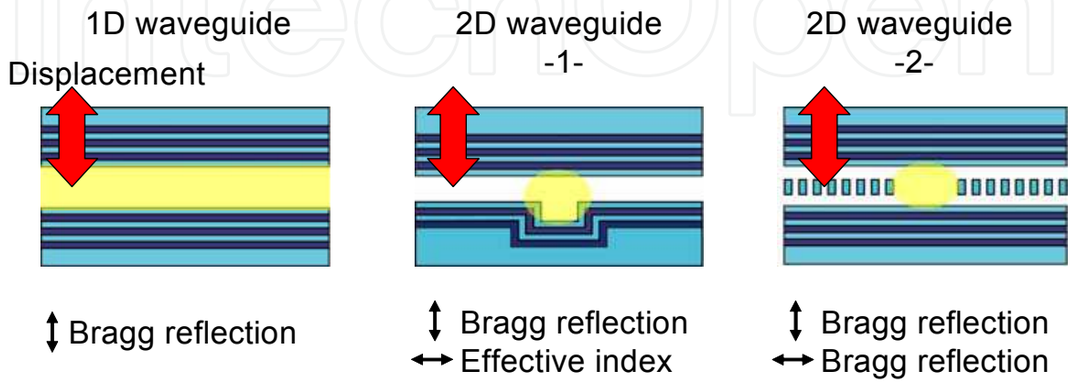

Fig. 3. Tunable Hollow optical waveguide structures [38]-[40].

differences generated by the air-gap steps or Bragg reflections due to periodic cladding structures just like vertical confinement. Tunable hollow waveguide structures are suitable for the temperature insensitive and widely tunable optical devices.

3.2 Propagation characteristics of tunable hollow waveguide

For the simplicity of the consideration, we assume the hollow waveguide composed of metal cladding. Metal-coated hollow waveguide is widely used in microwave or mili-wave frequency region. If the propagation loss of metal-coated 3D hollow waveguide is in an acceptable level, it can be used in our hollow waveguide devices. We investigate the propagation characteristics of metal coated 3D hollow waveguide in optical frequency region [24].

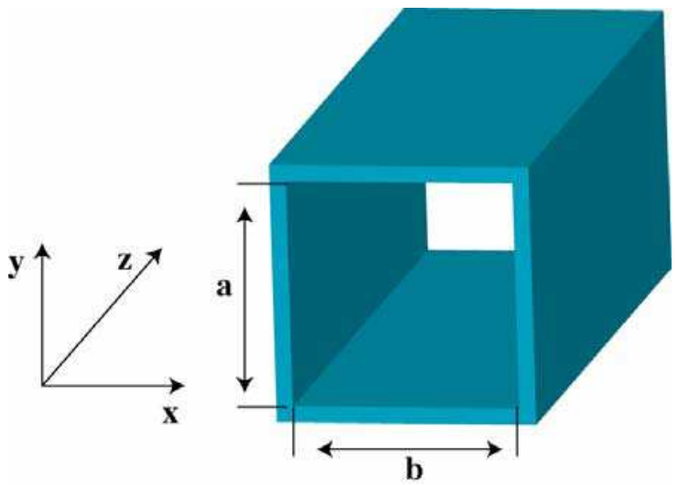

Fig. 4. Assumed 3D hollow waveguide model for analysis.

Assumed 3D hollow waveguide model for analysis is shown in Fig. 4. We have to derive the power flowing in the 3D hollow waveguide for determination of an attenuation factor. The flowing power Φ, which can be obtained by integrating the Poynting vector over transverse waveguide area of xy-plane, is expressed by

$$\Phi = \frac{1}{2} \cdot \mathrm{Re}\left[\int_0^a \int_0^b \left[E \times H^* \right]_z dxdy \right] \tag{1}$$

where $[E \times H^*]_z$ is the z-component of $[E \times H^*]$. We focus on TE_{10} mode that is expected as the mode of the lowest propagation loss. The power flow of TE_{10} mode can be expressed by

$$\Phi_{TE_{10}} = \frac{1}{4} \eta \left(\frac{2a}{\lambda} \right) \sqrt{1 - \frac{\lambda}{2a}} \cdot a \cdot b \cdot {H_0}^2 \tag{2}$$

where wave impedance: $\eta = (\mu/\varepsilon)^{1/2}$ and $E_x = 0$ is used.

The main factor of the propagation loss of a metallic hollow waveguide is ohmic loss in a metallic wall. If the electric conductivity is finite value, the electromagnetic wave penetrates into the inside of the metallic wall. The depth of this penetration, called *skin depth*, is expressed by

$$\delta = \frac{1}{\sqrt{\pi \cdot f \cdot \mu \cdot \sigma}} = \sqrt{\frac{2}{\omega \cdot \mu \cdot \delta}} \text{ [m]} \tag{3}$$

where f and δ is frequency and electric conductivity of metal, respectively.
Then faradic current is caused by the penetrate electromagnetic wave as shown in Fig. 5. Assuming magnetic field to be H_t, the surface current density can be expressed by

$$i_s = H_t \text{ [A/m]}. \tag{4}$$

It is thought that the surface current is flowing uniformly in the penetrate depth of δ. Therefore the ohmic loss for the unit area is expressed by

$$p = \frac{1}{2} i_s^2 R_s = \frac{1}{2} i_s^2 \sqrt{\frac{\pi \mu f}{\sigma}} \text{ [Ω]} \tag{5}$$

where R_s is surface resistance,

$$R_s = \frac{1}{\delta \cdot \sigma} = \sqrt{\frac{\pi \mu f}{\sigma}} \text{ [W/m2]}. \tag{6}$$

The total ohmic loss *P* can be obtained by sum of the ohmic loss *p* along all surrounding metallic wall for the unit length. Therefore the attenuation factor for the power flow can be expressed by

$$\alpha_p = \frac{P}{\Phi} \text{ [Neper/m]}. \tag{7}$$

The attenuation factor for the electric or magnetic field flow is also expressed by

$$\alpha_c = \frac{\alpha_p}{2} = \frac{P}{2\Phi}. \tag{8}$$

We derive the ohmic loss in surrounding metallic wall for TE10 mode.
The all of the surrounding ohmic loss for TE_{10} mode is given by the sum of p_1, p_2 and p_3. p_1 is the ohmic loss at the surface of y = 0, b resulting from the faradic current i_x, which is caused by H_z at the surface of metallic wall. p_2 is the ohmic loss at the surface of x = 0, a resulting from the faradic current i_y, which is caused by H_z at the surface of metallic wall. p_3 is the ohmic loss at the surface of y = 0, b originated from the faradic current i_z, which is caused by H_x at the surface of metallic wall. Each component of magnetic field can be obtained by solving Maxwell's equations as shown in [24].

$$\begin{aligned} H_x &= j\frac{a}{\pi} \cdot \beta_{01} \cdot H_0 sin\left(\frac{\pi x}{a}\right) \cdot \exp\left(-j\beta_{01} z\right) \\ H_y &= 0 \\ H_z &= H_0 \cdot \cos\left(\frac{\pi x}{a}\right) \cdot \exp\left(-j\beta_{01} z\right) \end{aligned} \tag{9}$$

where β_{01} is the propagation constant of TE_{01} mode.

$$\beta_{10} = k\sqrt{1-\left(\frac{\lambda}{2a}\right)^2} \tag{10}$$

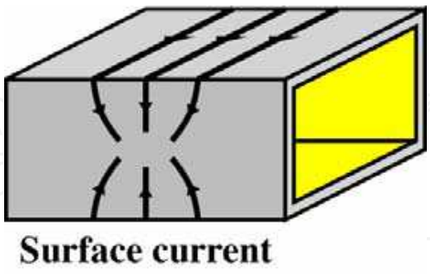

Fig. 5. Surface current caused by the penetration of electromagnetic waves.

The ohmic loss p_1, p_2 and p_3 can be expressed by

$$\begin{aligned} p_1 &= \int_0^a \left[\frac{1}{2}\left|i_x\right|_{y=0}\right|^2 R_s + \frac{1}{2}\left|i_x\right|_{y=b}\right|^2 R_s\Big]dx = \frac{1}{2}R_s H_0 a \\ p_2 &= \int_0^b \left[\frac{1}{2}\left|i_y\right|_{x=0}\right|^2 R_s + \frac{1}{2}\left|i_y\right|_{x=a}\right|^2 R_s\Big]dy = {H_0}^2 R_s b \\ p_3 &= \int_0^a \left[\frac{1}{2}\left|i_z\right|_{y=0}\right|^2 R_s + \frac{1}{2}\left|i_z\right|_{y=b}\right|^2 R_s\Big]dx = \frac{a^3}{2\pi^2}{\beta_{01}}^2 {H_0}^2 R_s \end{aligned} \tag{11}$$

Therefore the total ohmic loss is expressed by

$$P_{TE_{10}} = p_1 + p_2 + p_3 = \frac{1}{2}R_s H_0\left[a + 2b + \frac{a^3}{\pi^2}{\beta_{01}}^2\right]. \tag{12}$$

The attenuation factor for power flow can be described as

$$\alpha_{p_{TE10}} = \frac{P_{TE_{10}}}{\Phi_{TE_{10}}} = \frac{2R_s\left\{a + 2b + \frac{a^3}{\pi^2}{\beta_{10}}^2\right\}}{\eta ab\left(\frac{2a}{\lambda}\right)^2\sqrt{1-\left(\frac{\lambda}{2a}\right)^2}} \tag{13}$$

We can estimate the propagation loss of metallic hollow waveguide for the optical frequency region using eq. (13). The propagation loss for 20 x 20 μm hollow waveguide is as large as about 95 dB/cm at a wavelength of 1550 nm with gold walls. Even if the waveguide width is set to 100 μm, the propagation loss of about 19 dB/cm is expected. This propagation loss is too large to use in the optical devices.

The propagation constant of the light guided in the waveguide, shown in Fig. 6 can be expressed both for TE and TM mode as

$$\beta_{mn} = \sqrt{k^2 - \left[\left(\frac{m\pi}{D}\right)^2 + \left(\frac{n\pi}{W}\right)^2\right]} \tag{14}$$

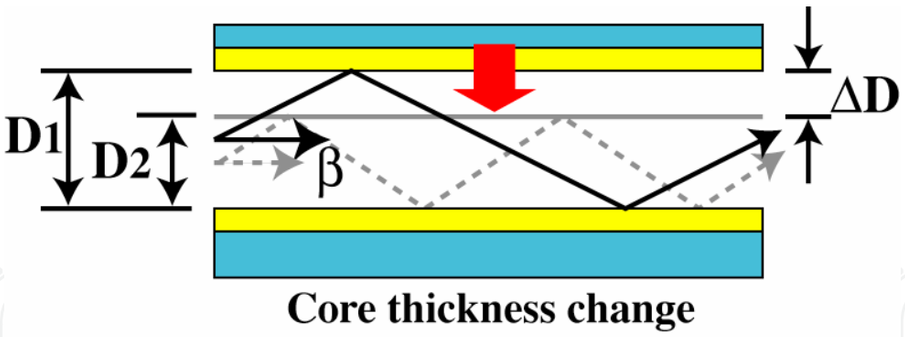

Fig. 6. Conceptual diagram of propagation constant tuning.

where m and n are mode number, k is wave vector in vacuum. This equation can be derived from Maxwell's equation [24]. We are now focusing on the case of the slab hollow waveguide; the width of the waveguide D becomes infinite. Therefore the propagation constant is independent of the mode number of n, since the light cannot form the mode for lateral direction. The propagation constant can be expressed as

$$\beta_m = k\sqrt{1-\left(\frac{m\lambda}{2D}\right)^2} \tag{15}$$

We rewrite this equation for a fundamental mode as

$$\beta_1 = k\sqrt{1-\left(\frac{\lambda}{2D}\right)^2} \tag{16}$$

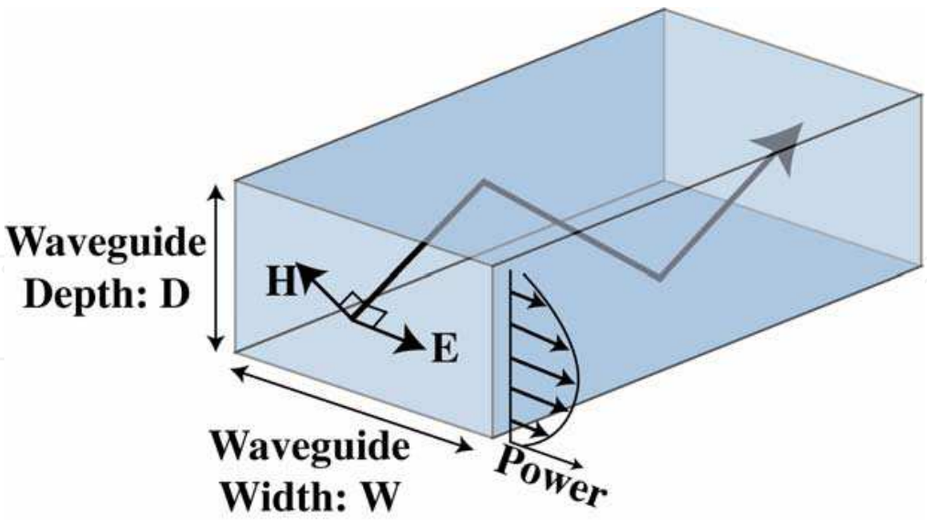

Fig. 7. Assumed model for analysis of propagation characteristics of hollow waveguide.

This equation shows the dependence of propagation constant of the guided fundamental mode on the air core thickness of the waveguide. From this equation, we can say that the propagation constant will be larger for larger values of waveguide thicknesses; the propagation constant is very sensitive to any change in the core thickness for the narrower

cores. The propagation constant in the hollow waveguide is smaller than that in free space, in other words, the effective refractive index becomes smaller than unity. It is to be noted that the phase velocity of the guided mode seems faster than that of the free space. However the propagated mode doesn't propagate faster than the light propagated in free space. The group velocity of the guided mode remains slower than that in the free space.

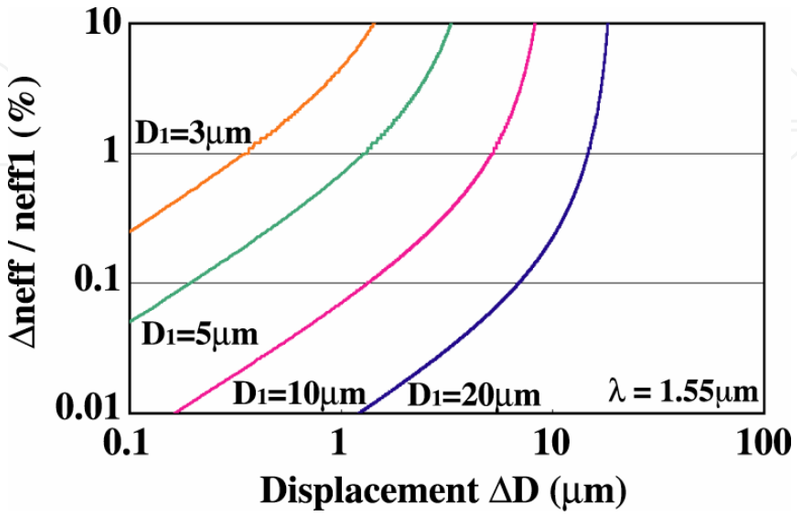

Fig. 8. Calculated effective refractive index change with the displacement of core thickness.

The calculated the effective refractive index change, namely change in propagation constant, is shown in Fig. 8. The effective refractive index change is plotted as a function of the displacement of the core thickness, when the core thickness changes from "initial thickness" to "initial thickness - ΔD" for the different initial thickness of 5, 10, 15 and 20 μm. The effective refractive index change diverges, when the displacement of the core thickness approaches to the initial core thickness. This can be understood from eq. (16). From Fig. 8, we can see that the effective refractive index change of few % can be expected. For example, when the core thickness is decreased from 5 μm to 3 μm, the effective refractive index change becomes as large as 2.2 %. It is difficult to achieve such a large number in conventional dielectric waveguides. This graph also shows that the change in effective refractive index becomes large as the range of the core thickness deviation becomes small. Therefore a narrow core hollow waveguide can effectively provide larger tuning.

4. Tunable 3D hollow waveguide

Hollow waveguides offer various interesting features including high power transmission, temperature insensitivity, low nonlinearity and strong optical confinement in comparison with conventional waveguides consisting of solid materials. In addition, waveguide type devices provide us the advantages in terms of miniaturization and integration of optical components and modules. These characteristics are very suitable for optical communication and sensing applications. Especially, the requirements of temperature insensitivity and wide tunability in optical components will become important along with the progress in future photonic networks. Our group has demonstrated a number of tunable optical devices based on slab hollow waveguides [25-27]. As shown in Fig. 3, the lack of lateral confinement in

slab hollow waveguide is not suitable for practical applications in integrated photonic circuits, especially for two port devices where spot size mismatch may be an issue. A 3D hollow waveguide can solve this problem and can be flexibly designed for number of functionalities [28].

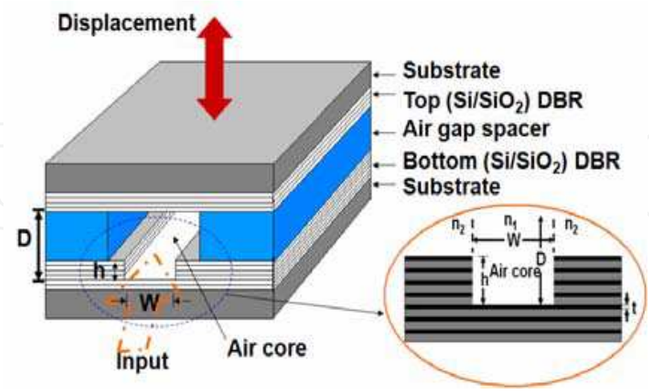

(a)

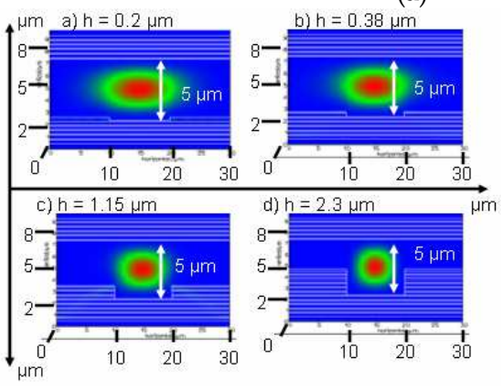

(b)

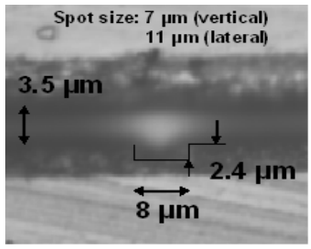

(c)

Fig. 9. (a) Schematic of tunable 3D hollow waveguide. All the layers in top and bottom DBR mirrors are quarter wavelength thick except the first silicon layer in bottom DBR just under the air core which we call phase matching layer with thickness *t*, shown in inset. (b) Computed effect of step-height on mode-field distributions at an air core thickness D = 5 μm and step width W = 10 μm, and (c) measured near field pattern for TE-mode.

The schematic of tunable 3D hollow waveguide is shown Fig. 9(a). The light is guided in the air with the help of two multilayer mirrors called distributed Bragg reflectors (DBRs). The vertical optical confinement is achieved by making the layers of DBR quarter wavelength thick for oblique incidence of light. For the lateral optical confinement, a groove is formed in the bottom DBR. The air core thickness will be larger in the region of this groove than in the lateral region. In view of eq. (16), larger air core thickness will have larger effective index. If the effective index of air core is n_1 and that of lateral air cladding is n_2 where $n_1 > n_2$ because of the difference in air gaps in lateral direction. The guided wave exhibits a difference in effective indices in the lateral direction, resulting in a lateral optical confinement by *quasi* total internal reflection. Thus, light can be laterally confined in the core region with a groove in one of the DBRs. In addition, the presence of groove, we call it a *step*, formed in one of the DBRs provides extra degree of freedom to control the propagation characteristics of hollow waveguide which can be tailored for a number of applications.

The lateral optical confinement and hence the lateral spot size can be varied with the step height *h*. The variation in TE-mode field distribution has been studied in Fig. 9(b) at an air core thickness of 5 μm with step width of 10 μm. Fig. 9(c) shows measured near field pattern for TE mode of the waveguide where the top DBR mirror of the 3D hollow waveguide with 2.4 μm deep and 8 μm wide groove is fabricated by electron-beam evaporation with 11 pairs of Si/SiO_2 on silicon substrate followed by inductive coupled plasma (ICP) -reactive ion etching (RIE). A strong optical confinement, in both vertical and lateral directions, can be achieved with the 3D hollow waveguide with a step formed in one of the two DBRs. The lateral optical confinement in hollow waveguides carries multifold benefit of efficient external coupling and wider tuning [29]. In following sections we will discuss the tailoring of hollow waveguide characteristics to realize important optical functionalities.

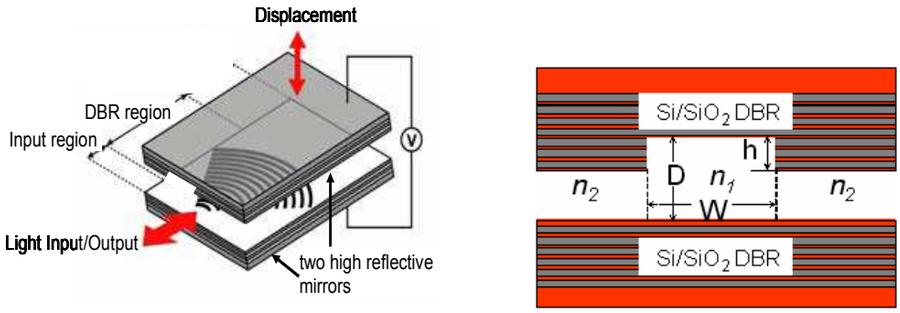

(a) (b)

Fig. 10. (a) Schematic of tunable Bragg reflector based on 3D hollow waveguide and (b) cross section of 3D hollow waveguide.

5. Tunable Bragg reflector based on 3D hollow waveguide

5.1 Bragg grating loaded hollow waveguide

The wide tuning in propagation constant, discussed in section 3, of hollow waveguide with variable can be utilized to make various tunable optical devices. One example of this can be a Bragg grating loaded hollow waveguide which shows a tuning in Bragg wavelength by varying the air core [25] which can be an important photonic building block for the realization of in-plane photonic integrated circuits. Fig. 10 shows a tunable Bragg reflector based on a 3D hollow waveguide. The top DBR is having a step formed in it for the lateral optical confinement and the bottom DBR is loaded with a circular grating.

The top and bottom DBRs provide vertical confinement in the air gap and the step in top DBR provides lateral confinement. The circular Bragg grating on the bottom DBR gives high reflection for Bragg wavelength which is decided, for first-order grating in slab hollow waveguide [25], by the following equation

$$\lambda_{Bragg} = 2 \cdot \left(\beta / k_0 \right) \cdot \Lambda \tag{17}$$

where Λ is grating pitch. Putting eq. (16) into (17) gives

$$\lambda_{Bragg} = 2 / \sqrt{(1/D^2) + (1/\Lambda^2)} \tag{18}$$

This eq. shows that Bragg wavelength can be tuned with a variable air core thickness.

5.2 Fabrication and characterization

The two DBRs used in hollow waveguide are fabricated by electron beam (EB) evaporation. A 2.3 µm deep and 10 µm wide step is formed in top DBR by dry etching followed by selective wet etching. To confirm the optical confinement in hollow waveguide, a measurement set up discussed in [25] is used. The measured near field pattern for TE mode was shown in Fig. 9(c). To form the Bragg reflector, a circular Bragg grating is fabricated using EB lithography followed by dry etching. The grating depth, pitch and length are 500 nm, 820 nm and 1 mm, respectively. The total device length is 3 mm.

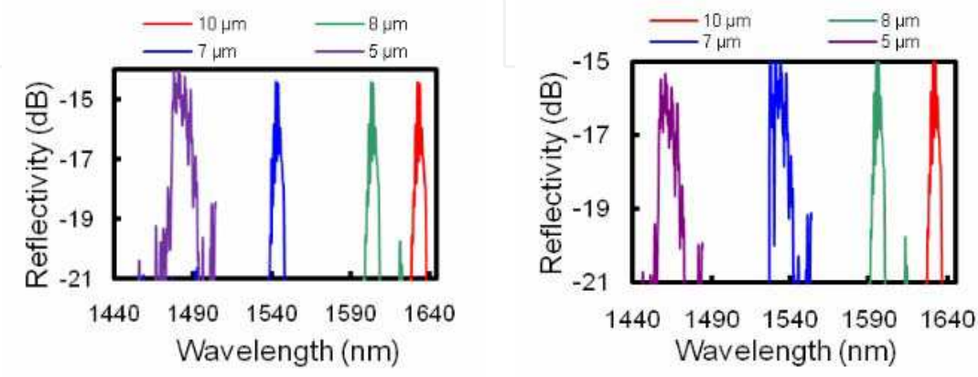

Fig. 11. Measured reflected spectra at various air core thicknesses of tunable Bragg reflector based on 3D hollow waveguide for (a) TE mode and (b) TM mode.

The same measurement set up of [25] is used to demonstrate the tuning in 3D hollow waveguide. As is clear from eq. (18), a variation in air core thickness D leads to a change in Bragg wavelength. The air core has been varied using an external piezoelectric actuator. The measured reflected spectra of TE and TM modes, at various air core thicknesses, are respectively shown in Fig. 11(a) and (b). The reflected spectra are measured at air core thicknesses of 10, 8, 7 and 5 µm. A clear blue-shift in the reflected spectra of the Bragg reflector, for both TE and TM modes, has been observed by decreasing the air core thickness from 10 µm to 5 µm. It is evident that a change in air core thickness can change the Bragg wavelength and hence a tunable Bragg reflector can be realized with hollow waveguide.

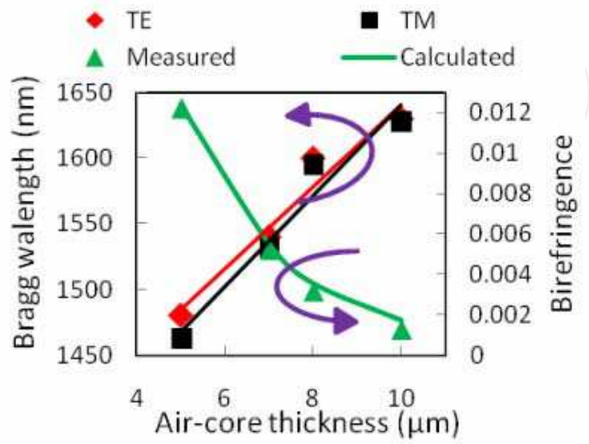

Fig. 12. Right y-axis: measured tuning in Bragg wavelengths with a variable air core for TE and TM modes. Left y-axis: measured tuning in birefringence by varying the air core thickness.

5.3 Tuning in Bragg wavelength and in birefringence

The measured Bragg wavelength as a function of air core thickness is shown in Fig. 12. By varying the air core thickness from 10 μm to 5 μm, a Bragg wavelength tuning of 152 nm for TE mode and that of 164 nm in TM mode are measured. Thus a grating loaded hollow waveguide can be used to provide giant tuning in Bragg wavelength which can find applications in realizing various tunable optical functions such as tunable filter, tunable lasers and so on. Further large tuning range can be achieved with narrower air core. The displacement of air core from smaller values of air core thicknesses results in larger tuning because of the tighter confinement. The reported tuning range is much larger than that in the tunable photonic devices based on the conventional dielectric waveguides using electro-optic and thermo-optic effects. Also, the tuning range is larger than that of slab hollow waveguide for the same displacement of air core because of the lateral optical confinement due to the presence of the step in top DBR [29]. Fig. 12 also shows how the modal birefringence can be tuned with variable air core thickness. The birefringence is defined by $B = (\lambda_{TE} - \lambda_{TM}) / \lambda_{TE}$, where λ_{TE} and λ_{TM} are the Bragg wavelengths of TE and TM modes, respectively. By varying the air core thickness from 5 μm to 10 μm, the birefringence decreases from 0.012 to 0.0012, providing a 900 % tuning and thereby making the 3D hollow waveguide a potential candidate to realize on-chip polarization control. The tunable birefringence can be useful for making tunable polarization manipulating devices.

6. Adjustable first-order polarization mode dispersion compensation

6.1 Giant birefringence from hollow waveguide

In long haul optical transmission systems, the degradation of transmitted optical signal from material and waveguide dispersion is a crucial problem. The dispersion, including polarization mode dispersion (PMD), is also a potential data rate limiting factor [30]. PMD occurs because of many intrinsic and extrinsic parameters including fiber core asymmetries, pressure, tension, vibration and temperature fluctuations, which lead to different transmission speeds of orthogonal polarizations causing random pulse distortion and pulse broadening in data stream; PMD becomes severe at increased data rates over 40 Gbit/s and higher [31]. To avoid the degradation of signal in fiber optic links, PMD compensation is necessary. A large birefringence and a tunable differential group delay (DGD) are needed to realize an adjustable PMD compensator, which can be achieved with a chirped Bragg grating filter to cancel the PMD in optical fibers [32]. A long fiber Bragg grating with some complicated tuning scheme is usually required to achieve large birefringence and a wide tuning in DGD [33]. An on-chip control of DGD with the tuning scheme other than the thermal tuning can be useful to realize a compact, temperature insensitive and low power consumption PMD compensator. Based on a tapered slab HWG, a planar Bragg reflector can provide chirping and an adaptable dispersion compensator can be realized [27]. In this section, we show that a giant birefringence can be realized with a 3D HWG by optimizing the step-height. A tapered-3D-HWG-Bragg-reflector has been proposed in which DGD can be tuned by varying the taper angle.

The schematic side-view of tunable Bragg reflector based on a 3D HWG is shown in Fig. 13(a), in which a step, of height *h* and width *W*, has been formed in a top DBR while the bottom DBR is loaded with a SiO_2 grating. The cross-section of the 3D hollow waveguide was shown in Fig. 10(b). The quarter wavelength thick top and bottom multilayer (DBR) mirrors provide strong optical confinement in vertical direction. Fig. 13(b) shows the effect

of step height on the birefringence which is defined by $B = (\beta_{TE} - \beta_{TM}) / \beta_{TE}$, where β is propagation constant. The birefringence increases with increasing step-height because of the increase in lateral effective index contrast which was shown in Fig. 9(b). The calculated birefringence at a step-height of 2.3-μm is 0.012 with 5-μm thick air core. This giant birefringence, which is two orders of magnitude larger than that with other conventional fiber based technologies, can provide us compact devices with efficient functionality for PMD compensation etc.

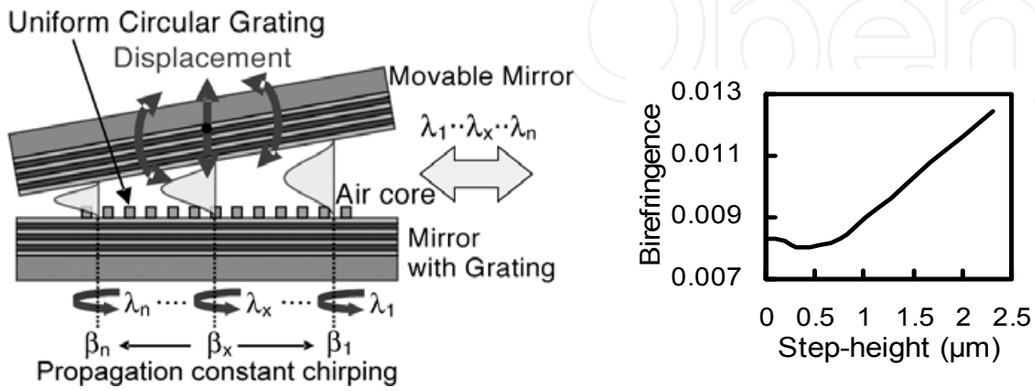

Fig. 13. (a) Schematic of tapered 3D hollow waveguide Bragg reflector (b) calculated birefringence (of straight hollow waveguide) versus step height *h* at an air core thickness D = 5 μm and step width W = 10 μm.

For the fabrication of tunable Bragg reflector based on 3D hollow waveguide, the top and bottom Si/SiO_2 multilayer mirrors have been prepared by electron beam (EB) evaporation. The 2.3-μm deep and 10-μm wide step is formed, in the top DBR mirror, by dry etching followed by selective wet etching. The grating has been fabricated, on the bottom DBR by electron-beam lithography followed by dry etching. The grating depth, pitch and length are 500 nm, 860 nm and 1 mm, respectively; and the total device length is 3 mm. The larger step-height, discussed above, carries multifold benefits of increased birefringence and reduced spot size because of increase in lateral index contrast. Also, The grating coupling coefficient is largest around 2.3-μm, which can broaden the reflection-band of the Bragg reflector [28], an important requirement to define a constant wavelength of operation of the device for two orthogonal polarizations.

6.2 Demonstration of tunable DGD

The dispersion and hence the group delay in hollow waveguides can be enhanced by introducing a taper. The large birefringence causes a delay between TE and TM modes of the 3D HWG; and the variable taper-angle can enhance the group delays and delay difference between these two orthogonal polarizations. The measured reflected spectra of TE and TM modes at various taper angles are shown respectively in Fig. 14(a) and (b). The broadband reflection of both the polarizations is obtained which is because of the combined effect of optimized 3D hollow waveguide and tapering. An overlap between the reflection-bands of TE and TM modes has also been observed. The taper angle has been varied from -0.038˚ to 0.057˚. The taper-angle 0˚ refers to the straight 3D hollow waveguide (without taper). Increasing the taper-angle has the effect on reflection bandwidths of TE and TM modes; the bandwidth increases by increasing the taper-angle, because of the increased

spatial chirping in Bragg wavelength. The net insertion loss remains less than 2.5 dB for 3-mm long device.

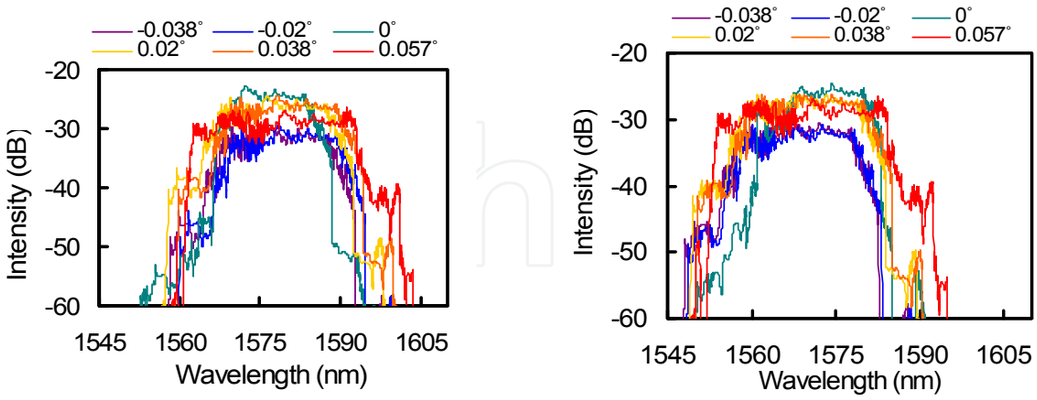

(a) (b)

Fig. 14. Measured reflection spectra of tapered 3D hollow waveguide Bragg reflector for (a) TE mode and (b) TM mode.

In hollow waveguides, because of air core guiding, the angle of incidence of fundamental mode is smaller than Brewster's angle which makes the orthogonal polarizations out of phase causing large polarization dependence. Also, the presence of a step in one of the multilayer mirrors affects the orthogonal polarizations and polarization dependence can be further increased by varying the step-height. As shown in Fig. 13(b), by increasing the step-height, birefringence can be increased; an ultrahigh birefringence of 0.012, much larger than that of the slab HWG (step-height h = 0), can be achieved in a straight 3D HWG with a 2.3-μm high and 10-μm wide step at a 5-μm thick air core. The measured birefringence of the 3D hollow waveguide Bragg reflector as a function of taper-angle is shown in Fig. 15(a); where birefringence is defined by $B = (\lambda_{TE} - \lambda_{TM}) / \lambda_{TE}$, where λ is the center Bragg wavelength. A small variation in birefringence has been observed by varying the taper angle. The birefringence is less dependent on the taper angle; the birefringence remains around 0.01, which is in agreement with the Fig.13(a), and is almost two-order of magnitude larger than the birefringence of fiber Bragg gratings.

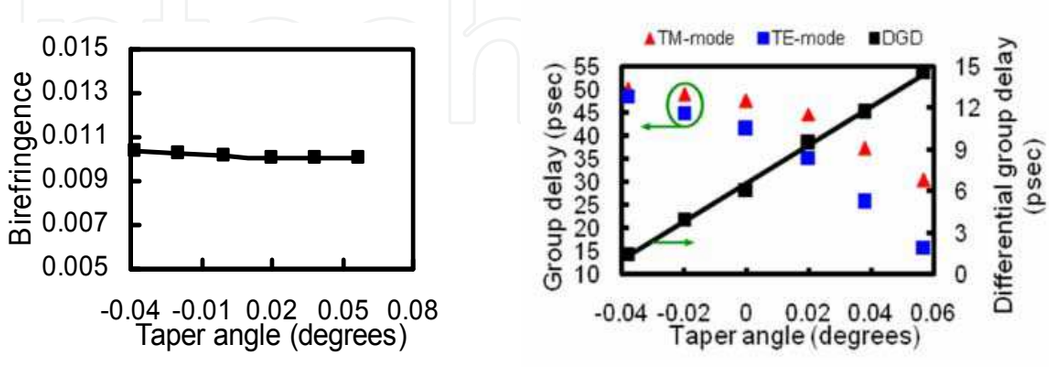

(a) (b)

Fig. 15. (a) Measured birefringence versus taper-angle and (b) measured group delays of TE and TM modes, and DGD as a function of taper-angle.

The measured group delays of TE and TM modes of the Bragg reflector based on tapered 3D hollow waveguide, at various taper-angles, are shown in Fig. 15(b). By increasing the taper-angle, group delay, for both the polarizations, increases because of the enhancement of chirping in propagation constant of the guided mode. The increasing taper-angle has larger effect on TE polarization than that on TM polarization. Thus at larger taper-angles, the difference between group delays of TE and TM modes becomes larger which causes a tuning in DGD, where DGD is defined as the difference of group delays between TE and TM modes. Fig. 15(b) also shows tuning in DGD as a function of taper-angle; increasing the taper angle from -0.038˚ to 0.057˚, DGD increases from 1.5-psec to 14.6-psec, providing us a 13.1-psec tuning in DGD, with a 3-mm long compact device. The large birefringence and tunable DGD of the proposed compact 3D HWG Bragg reflector makes it a good candidate for dynamic adjustable compensation of PMD in high bit rate and high speed transmission in optical fiber links. The giant birefringence can be used in tunable polarization manipulating devices based on a tunable 3D hollow waveguide.

7. Future prospects

7.1 Integration technology for tunable hollow waveguide devices

Hollow waveguides offer various interesting features including temperature insensitivity and ultra wide tuning. The design of hollow waveguide is flexible which carries the possibility of implementation of other functionalities in hollow waveguides. For efficient coupling of a hollow waveguide with a single mode fiber, a spot size converter may be used [26]. Fig. 16 shows how the tunable hollow waveguide can be implanted to realize reconfigurable photonic integrated circuit using high index core loaded waveguides for WDM applications. A spot size converter can be used for coupling to ultra-widely tunable functional devices consisting of hollow waveguide with sub-micron air core. And then, high index core loaded non-taper waveguides can be used as connecting waveguides between tunable devices or input/output waveguides to hollow waveguide devices. This kind of circuit is shown in Fig. 16.

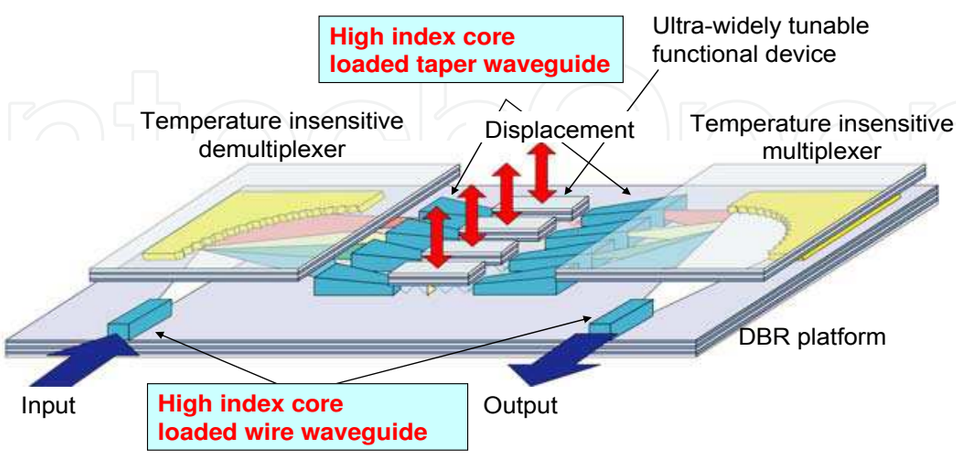

Fig. 16. Image of the scheme of reconfigurable photonic integrated circuit with tunable hollow waveguide using a high index core loaded waveguides for WDM applications.

The limiting factor of the tuning range has resulted from the alignment accuracy of air gap between two multilayer mirrors used as hollow waveguide cladding. This difficulty could be overcome by replacing a PZT actuator with a monolithic MEMS actuator. For this purpose a tunable hollow waveguide Bragg reflector with monolithically integrated MEMS electro-thermal actuator is shown in Fig. 17 [34]. This concept for hollow waveguide integration would enable to realize the tunable optical devices such as tunable lasers and tunable filters etc. with ultra-wide tuning and temperature insensitivity at the same time.

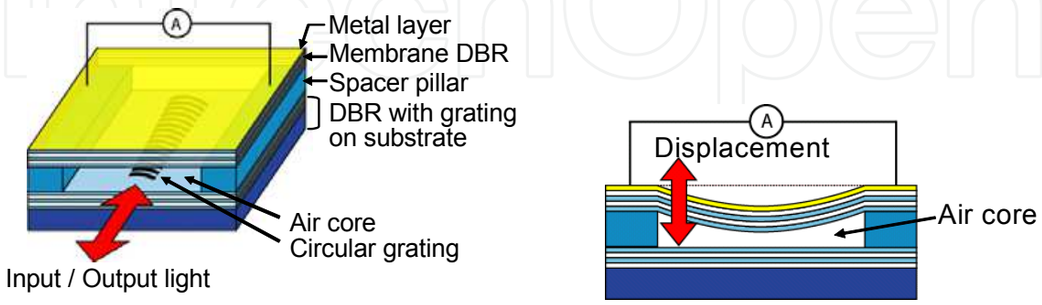

(a) (b)

Fig. 17. Schematic structure of tunable hollow waveguide Bragg reflector with integrated electro-thermal actuator. (a) Bird's-eye and (b) cross-sectional views.

7.2 Hollow waveguide with DBR and high index contrast grating: Extra degree of freedom for on-chip polarization control

As discussed in previous sections, the strong vertical optical confinement in hollow waveguides (HWGs) can be achieved using top and bottom DBRs as cladding, having quarter wavelength thick layers designed for oblique incidence of light, where light is guided in the air gap in between the two DBRs. The reflectivity of DBRs in the HWG is highly polarization dependent because of the periodicity only in one direction. The polarization dependence of a HWG becomes very large at a narrow air core where a HWG offers giant tuning of over 10% in propagation constant.

The birefringence of the HWG largely comes from the guiding DBR having periodicity only in the one direction. If a lateral periodicity (perpendicular to both, the direction of propagation and the direction of DBR periodicity) is introduced in the HWG, the polarization dependence of the HWG can be reduced. High reflectivity DBRs can be replaced with a high contrast grating (HCG) mirror which gives broadband high reflection [28, 29]. The HCG mirror can be introduced, as a lateral periodicity, in hollow waveguides to reduce its birefringence. The combined (and opposite) effect of DBR (vertical periodicity) and HCG (lateral periodicity) enable us to reduce birefringence even at a narrow air core.

In this section, a hollow waveguide with vertical and lateral periodicity is proposed which consists of a DBR mirror as vertical periodicity and an HCG mirror as lateral periodicity. We show that the combination of DBR and HCG mirrors can provide strong optical confinement and can reduce the birefringence of the hollow waveguide with narrow air-cores.

The schematic of the proposed hollow waveguide is shown in Fig. 18(a). It consists of a DBR as a bottom mirror and a high index contrast grating (HCG) as a top mirror of a hollow waveguide. Light can be confined vertically in an air-core utilizing the high reflectivities of

DBR and HCG. The structure consists of a 5 pairs Si/SiO_2 bottom DBR mirror where each layer in DBR is quarter wavelength thick, which is designed for oblique incidence. Because of the high refractive index contrast between Si and SiO_2, only 5-pairs Si/SiO_2 are enough to achieve a high reflectivity. The top HCG mirror consists of a high index contrast silicon/air grating. In an HCG mirror, many in-plane reflections add up and give rise to vertical high reflection [18]. The design parameters for the hollow waveguides are: air core thickness D, grating thickness t_g, grating pitch Λ, grating teeth width w and grating duty cycle C. The calculated mode field distributions of TE mode in the hollow waveguide is shown in Fig. 18(b). A strong vertical confinement is observed in the hollow waveguide. The propagation loss at Λ = 1.2 μm, C = 0.41 and t_g =0.45 μm is 0.55dB/cm foe TE mode and that of TM mode is 2.7 dB/cm, at an air core thickness of 5μm which is acceptable for millimeter long waveguide devices. The set of the optimized parameters with D = 5 μm, t_g =0.45 μm, Λ = 1.2 μm, w = 0.5 μm and C = 0.41 is called "set A" for convenience.

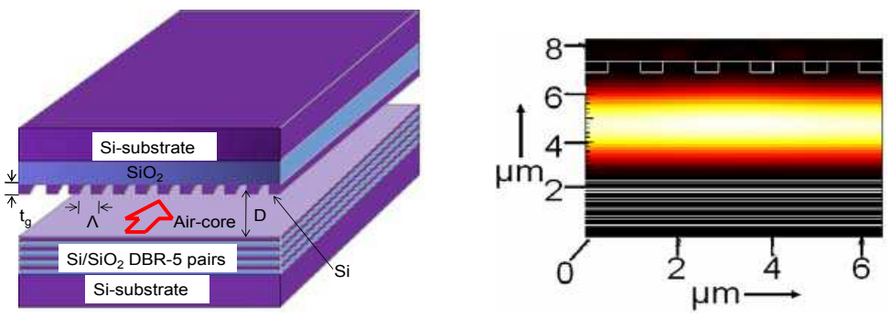

Fig. 18. (a) Schematic of hollow waveguide with DBR and HCG and (b) computed TE-mode distribution.

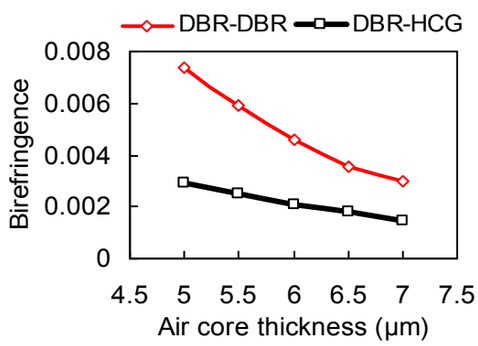

Fig. 19. birefringence as a function of D at the grating parameters in "set A", also shown birefringence of hollow waveguide with DBR on the both sides.

Hollow waveguides show large polarization dependence because of the shallow incidence angle of a fundamental mode. To realize ultra wide tuning in hollow waveguides, we need to use a hollow waveguide with a narrower air core; but the birefringence at narrower cores remains large. The polarization characteristics of HCG hollow waveguides are shown in terms of birefringence in Fig. 19 at the grating parameters of "set A". The birefringence is defined as $B = (\beta_{TE} - \beta_{TM}) / \beta_{TE}$, where β is propagation constant. In Fig. 19, the effect of an air core on the birefringence is shown where the birefringence of conventional hollow

waveguides (having DBRs on top and bottom) is also shown for comparison. The result shows that the birefringence of the HCG hollow waveguide is smaller than that of the conventional hollow waveguide at narrower air cores. By increasing the air core thickness, the birefringence of the hollow waveguides decreases for both the cases. At an air core thickness of 5 μm, the birefringence of the HCG hollow waveguide is 2.8×10^{-3}; which is almost 2.6-times smaller than the birefringence of a conventional hollow waveguide. To achieve ultra wide tuning, the HCG hollow waveguide with narrower air-cores can be realized with smaller birefringence. The reason for this small birefringence is because of the opposite nature of conventional DBR mirror and HCG mirror; their combined (and opposite) interaction with the orthogonal polarizations results in the reduced birefringence. In case of the DBR-DBR HWG, the large birefringence comes from the field penetration of a TM mode into the DBR. The propagation constant of a TM mode is larger than that of a TE mode. On the other hand, a HCG gives us stronger optical confinement for a TM mode in an air core than DBRs. Thus, the propagation constant of a TM mode in the HCG-DBR HWG is smaller than that in the DBR-DBR HWG while the propagation constant of a TE mode remains almost same for both the cases. The difference in the field penetration results in a reduced birefringence.

The birefringence and the polarization dependence loss can be reduced with the further optimizations of the grating and the waveguide parameters [17]. The introduction of HCG into hollow waveguides can extend the fabrication tolerance of the structure because of the large fabrication tolerance of HCG and it can provide the lateral optical confinement as well [17]. Also, because of the ease of fabrication of HCG, it is possible to design it for one particular polarization, making polarization control very flexible. With the flexibility of HCG-design, it is possible to build hollow waveguides with widely tunable polarization nature for variety of applications. With the collaboration of HCG and the inherent properties of hollow waveguides such as temperature insensitivity and wide tuning, it will be possible to design novel tunable optical functions with large design tolerances.

8. References

[1] Pochi Yeh and Amnon Yariv, "Bragg reflection waveguides", *Opt. Commun.* 19, 427 (1976).

[2] M. Ibanescu, Y. Fink, S. Fan, E.L. Thomas and J.D. Joannopoulos, "The coaxial omniguide - a novel all- dielectric waveguide", *Science* 89 (2000) 415.

[3] M.A. Duguay, Y. Kokubun, T. Koch, and L. Pfeiffer, "Antiresonant reflecting optical waveguides in SiO_2-Si multilayer structures," *Appl. Phys. Lett.* 49, 13-15 (1986).

[4] R. F. Cregan, B. J. Mangan, J. C. Knight, T. A. Birks, P. St. J. Russell, P. J. Roberts, and D. C. Allan: *Science* 285 (1999) 1537.

[5] H. Schmidt, D. Yin, J. P. Barber, and A. R. Hawkins: *IEEE J. Select. Topics Quantum Electron.* 11 (2005) 519

[6] M. Miyagi, A. Hongo, and S. Kawakami: *IEEE J. Quantum Electron.* QE-19 (1983) 136.

[7] T. Miura, F. Koyama, Y. Aoki, A. Matsutani, and K. Iga: Jpn. J. Appl. Phys. 40 (2001) L688.

[8] T. Miura, F. Koyama, and A. Matsutani: IEEE Photonics Technol. Lett. 15 (2003) 1240.

[9] J. Roberts, D. P. Williams, F. Couny, M. Lawman, M. Mason, S. Coupland, R. Flea, and H. Sabert: Proc. Optical Fiber Communications Conf., California, 2004, PDP24.

[10] V.R. Almeida, Q. Xu, C.A. Barrios, and M. Lipson, "Guiding and confining Light in void nanostructure," *Optics Letters* 29 pp. 1209-1211, 2004.
[11] D. G. Ouzounov, F. R. Ahmad, D. Muller, N. Venkataraman, M. T. Gallagher, M. G. Thomas, J. Silcox, K. W. Koch, And A. L. Gaeta: *Science* 301 (2003) 1702.
[12] J. D. Shephard, J. D. C. Jones, D. P. Hand, G. Bouwmans, J. C. Knight, P. St. J. Russell, and B. J. Mangan: *Opt. Express* 12 (2004) 717.
[13] J. C. Petersen, T. Sorensen, T. P. Hansen, and H. R. Simonsen: *Opt. Express* 12 (2004) 4080.
[14] V. Dangui, H. K. Kim, M. J. F. Digonnet, and G. S. Kino: Proc. Optical Fiber Communications Conf., Anaheim, 2005, OTuI4.
[15] Y. Sakurai, Y. Yokota, A. Matsutani, and F. Koyama: Proc. Optical Fiber Communications Conf., Anaheim, 2005, OME30.
[16] Y. Sakurai, Y. Yokota, A. Matsutani, and F. Koyama: Appl. Phys. Lett. (2005) 071111.
[17] M. Kumar, C. Chase, V. Karagodsky, T. Sakaguchi, F. Koyama, and C. J. Chang-Hasnain, "Low birefringence and 2-D optical confinement of Hollow waveguide with distributed Bragg reflector and high index contrast grating", *IEEE Photonics Journal 1*, No. 2, 135 (2009).
[18] M. C. Y. Huang, Y. Zhou, and C. J. Chang-Hasnain, "A surface-emitting laser incorporating a high-index-contrast subwavelength grating", *Nature Photonics* 1 (2007) 119.
[19] Y. Zhou, V. Karagodsky, Bala Pesala, F. G. Sedgwick, and C. J. Chang-Hasnain, "A novel ultra-low loss hollow-core waveguide using subwavelength high-contrast gratings," Optics Express 17 (2009) 1508.
[20] T. Miura, F. Koyama, and A. Matsutani: *Jpn. J. Appl. Phys.* 41 (2002) 4785.
[21] T. Miura, F. Koyama, and A. Matsutani: *Jpn. J. Appl. Phys.* 41 (2002) 5607.
[22] T. Miura and F. Koyama: Proc. Optoelectronics and Communications Conference/ International Conference on Optical Internet, Yokohama, 2004, 892.
[23] M. Kumar and F. Koyama, "Investigation and theoretical analysis of low-loss 3D hollow waveguides for widely tunable photonic devices", *Jpn. J. Appl. Phys.* 47 (2008) pp 3471-3475.
[24] T. Sekiguchi: *Electro-Magnetic Wave* (Asakura-shoten, Tokyo, 1976).
[25] Y. Sakurai and F. Koyama: "Tunable hollow waveguide Bragg reflectors with variable air core," *Optics Express* 12 (2004) 2851.
[26] Y. Sakurai and F. Koyama: "Modeling of a low-loss spot size converter for hollow waveguide with sub-wavelength air core", *IEICE Elect. Express* 1 (2004) 115-119.
[27] Y. Sakurai, A. Matsutani, and F. Koyama, *Applied Physics Letters*. 88 (2006) 121103.
[28] M. Kumar, T. Sakaguchi, and F. Koyama, "Giant birefringence and tunable differential group delay in Bragg reflector based on tapered three-dimensional hollow waveguide", *Applied Physics Letters* 94, Issue 6, 061112 (2009).
[29] M. Kumar, T. Sakaguchi, and F. Koyama, "Wide tunability and ultralarge birefringence with 3D hollow waveguide Bragg reflector", *Optics Letters* 34 (2009) 1252.
[30] T. Takahashi, T. Imai, and M. Aiki, Electron. Lett. 30, 348 (1994).
[31] Xia Zhang, Yuehui Xia, Yongqing, and Xiaomin Ren, Optics Commun. 214, 123 (2002).

[32] S. Lee, R. Khosravani, J. Peng, V. Grubsky, D. S. Starodubov, A. E. Willner, and J. Feinberg, IEEE Photon. Technol. Lett. 11, 1277 (1999).
[33] X. Yi, C. Lu, X. Pang, W. –D. Zhong, F. Wei, and Y. Fang, Opt. Express 11, 2634 (2003).
[34] F. Koyama, T. Miura and Y. Sakurai, IEICE Trans. Electron. J88-C (2005) 388.

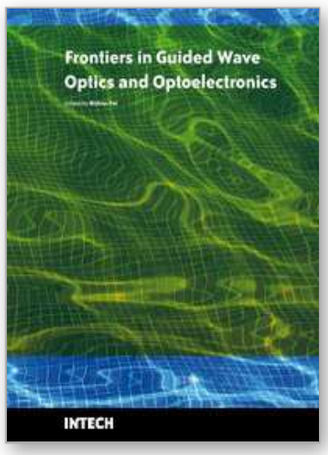

Frontiers in Guided Wave Optics and Optoelectronics

Edited by Bishnu Pal

ISBN 978-953-7619-82-4
Hard cover, 674 pages
Publisher InTech
Published online 01, February, 2010
Published in print edition February, 2010

As the editor, I feel extremely happy to present to the readers such a rich collection of chapters authored/co-authored by a large number of experts from around the world covering the broad field of guided wave optics and optoelectronics. Most of the chapters are state-of-the-art on respective topics or areas that are emerging. Several authors narrated technological challenges in a lucid manner, which was possible because of individual expertise of the authors in their own subject specialties. I have no doubt that this book will be useful to graduate students, teachers, researchers, and practicing engineers and technologists and that they would love to have it on their book shelves for ready reference at any time.

InTech Europe
University Campus STeP Ri
Slavka Krautzeka 83/A
51000 Rijeka, Croatia
Phone: +385 (51) 770 447
Fax: +385 (51) 686 166
www.intechopen.com

InTech China
Unit 405, Office Block, Hotel Equatorial Shanghai
No.65, Yan An Road (West), Shanghai, 200040, China
中国上海市延安西路65号上海国际贵都大饭店办公楼405单元
Phone: +86-21-62489820
Fax: +86-21-62489821

IntechOpen